Assessing EUV Mask Defectivity

Uzodinma Okoroanyanwu,[1] Anna Tchikoulaeva,[2] Paul Ackmann,[3] Obert Wood,[1] Bruno La Fontaine,[4] Karsten Bubke,[5] Christian Holfeld,[5] Jan Hendrik Peters,[5] Sumanth Kini,[6] Sterling Watson,[6] Isaac Lee,[6] Bo Mu,[6] Philip Lim,[6] Sudhar Raghunathan,[7] and Carol Boye.[7]

[1]GLOBALFOUNDRIES, 257 Fuller Road, Suite 3100, Albany NY 12203, USA
[2]GLOBALFOUNDRIES, Wilschdorfer Landstrasse 101, D-01109 Dresden, Germany
[3]GLOBALFOUNDRIES, 5113 Southwest Parkway, M/S 630, Austin, TX 78735
[4]GLOBALFOUNDRIES, 1050 E. Arques Avenue, Sunnyvale CA 94085, USA
[5]AMTC, Rahnitzer Allee 9, D-01109 Dresden, Germany
[6]KLA-Tencor, 255 Fuller Road, Suite 3100, Albany NY 12203, USA
[7]IBM, 257 Fuller Road, Suite 3100, Albany NY 12203, USA

ABSTRACT

This paper assesses the readiness of EUV masks for pilot line production. The printability of well characterized reticle defects, with particular emphasis on those reticle defects that cause electrical errors on wafer test chips, is investigated. The reticles are equipped with test marks that are inspected in a die-to-die mode (using DUV inspection tool) and reviewed (using a SEM tool), and which also comprise electrically testable patterns. The reticles have three modules comprising features with 32 nm ground rules in 104 nm pitch, 22 nm ground rules with 80 nm pitch, and 16 nm ground rules with 56 nm pitch (on the wafer scale). In order to determine whether specific defects originate from the substrate, the multilayer film, the absorber stack, or from the patterning process, the reticles were inspected after each fabrication step. Following fabrication, the reticles were used to print wafers on a 0.25 NA full-field ASML EUV exposure tool. The printed wafers were inspected with state of the art bright-field and Deep UV inspection tools. It is observed that the printability of EUV mask defects down to a pitch of 56 nm shows a trend of increased printability as the pitch of the printed pattern gets smaller – a well established trend at larger pitches of 80 nm and 104 nm, respectively. The sensitivity of state-of-the-art reticle inspection tools is greatly improved over that of the previous generation of tools. There appears to be no apparent decline in the sensitivity of these state-of-the-art reticle inspection tools for higher density (smaller) patterns on the mask, even down to 56nm pitch (1×). Preliminary results indicate that a blank defect density of the order of 0.25 defects/cm^2 can support very early learning on EUV pilot line production at the 16 nm node.

Keywords: EUV lithography, EUV blank and mask defects, defect printability

Extreme Ultraviolet (EUV) Lithography, edited by Bruno M. La Fontaine, Proc. of SPIE Vol. 7636, 76360J · © 2010 SPIE · CCC code: 0277-786X/10/$18 · doi: 10.1117/12.847348

Downloaded from SPIE Digital Library on 31 Mar 2010 to 192.146.1.254. Terms of Use: http://spiedl.org/terms

1. INTRODUCTION

Mask defectivity is one of the main remaining challenges yet to be satisfactorily resolved, before the implementation of EUV lithography in high volume manufacturing. There are three main categories of EUV mask defects:[1] blank defects embedded in the reflective multilayer blank, hard defects resulting from absorber patterning, and soft defects resulting from contamination during mask handling and use. The different types of defects associated with the above three categories behave differently during the patterning process due either to phase shift or amplitude modulation introduced by a defect in the proximity of patterned features. Of the many types of mask defects in the above three categories, the critical ones are those that are printable on the wafer. Termed repeaters, these printable mask defects are identified by their occurrence in the same location on multiple dies on the wafer. To this end, this paper investigates wafer printability of well characterized reticle defects, with particular emphasis on those reticle defects that cause electrical errors on wafer test chips.

In a previous study based on a reticle we call Gremlin1,[2] we reported the following: (1) that about 7% of 32 nm module and 45 % of 22 nm module blank defects are printable on the wafer; (2) that the blank defect printability increases as the pitch of the printed patterns gets smaller; (3) that some printable blank defects were detected neither during reticle nor wafer-inspection; (4) that reticle inspection sensitivity with older generation tools degrades as the pattern pitch gets smaller; (5) that the ability to detect defects on the wafer degrades as the blank defect size decreases.

In this study, we extend the work we did on Gremlin1 reticle defects to a newer generation reticle called Gremlin2, which has the same design as the former reticle, but was fabricated on a blank that had about five-fold fewer defects than Gremlin1, and whose absorber thickness is significantly smaller than that of Gremlin1.

In order to determine whether specific defects originate from the substrate, the multilayer film, the absorber stack, or from the patterning process, the reticles are inspected after each fabrication step. Following fabrication, the reticles were used to print wafers on a 0.25 NA full-field EUV exposure tool (ASML Alpha Demo Tool) in Albany NanoTech. Correlations between the blank, reticle and wafer inspection and SEM review results were used to establish the origins of the printable defects. Comparisons between results obtained with different blank and reticle inspection tool-sets were done with a view to determining the capabilities of each tool-set. Unless otherwise indicated, all the values used in this paper are scaled to the wafer level (1×).

2. EXPERIMENTAL

Two reticle test chips, Gremlin1 and Gremlin2, with the same design were used in this study. The blanks for these reticles were obtained from Asahi Glass Company, and the fabrication of the reticles was done at AMTC. The main differences between the two reticles is the fact that the blank used in Gremlin1 had 1.3 defects/cm^2, while that of Gremlin2 had 0.25 defects/cm^2. Also, the Gremlin2 absorber thickness is smaller than that of Gremlin1. The layout of the reticles is shown in Figure 1. Each of the reticle comprises a 10×13 arrays of defect monitors with three modules of serpentine and comb structures: 32 nm ground rule module (with pitch = 104 nm), 22 nm ground rule module

Downloaded from SPIE Digital Library on 31 Mar 2010 to 192.146.1.254. Terms of Use: http://spiedl.org/terms

(with pitch = 80 nm), and 16 nm ground rule module (with pitch = 56 nm). Each defect monitor array is 1 cm × 1 cm, and has both vertically and horizontally oriented structures (see Figure 2). The blanks were each inspected with Lasertec and Siemens DF-40X tools. The reticles were inspected with KLA-Tencor TeraScanHR and Teron 6xx series tools. Defect review was done with Scanning Electron Microscopes.

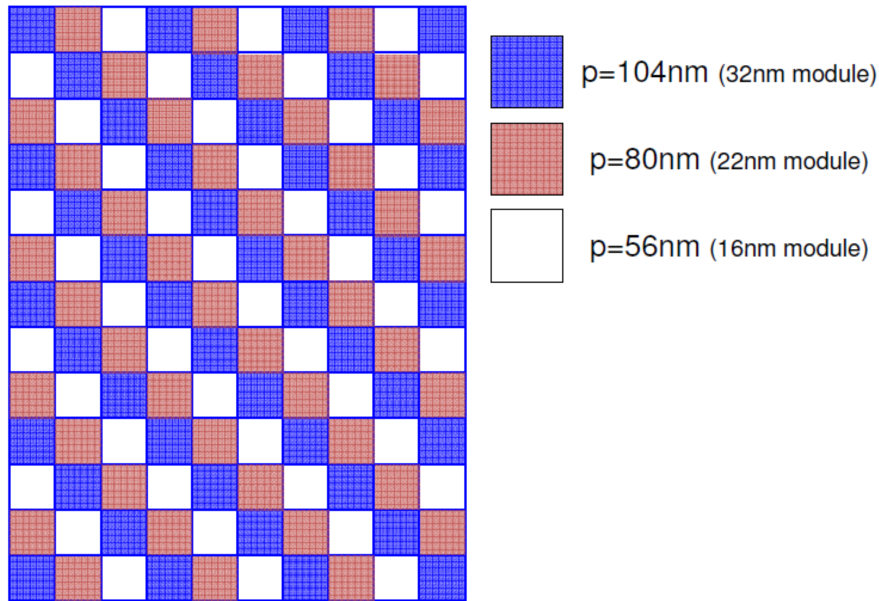

Figure 1. Layout of the Gremlin 1 and Gremlin 2 reticles. The reticle comprises three modules: 32 nm module (with pitch = 104 nm), 22 nm module (with pitch = 80 nm), and 16 nm module (with pitch = 56 nm).

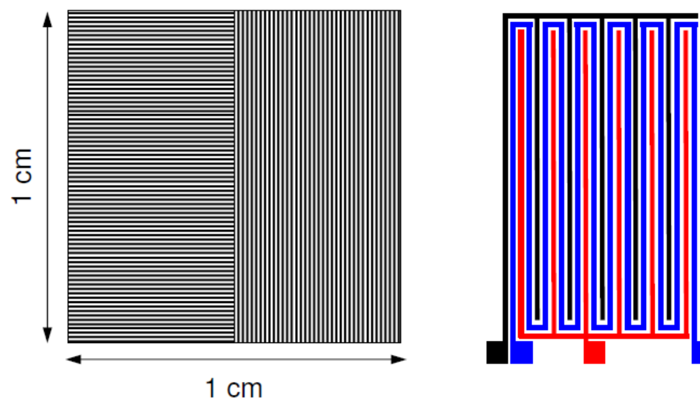

Figure 2. Layout of (A) horizontal and vertical features and (B) comb and serpentine structures of Gremlin mask.

Downloaded from SPIE Digital Library on 31 Mar 2010 to 192.146.1.254. Terms of Use: http://spiedl.org/terms

Resist exposure using these reticles was done on an ASML ADT with NA = 0.25, σ = 0.5. The resists used were SEVR40 and SEVR139, respectively, with a thickness of 100 nm and 75 nm, respectively. Wafer exposures were first done with Gremlin1 reticle with a well controlled process (across field CD uniformity ~ 1.3-1.5 nm, 3σ; line edge roughness ~ 3 nm, 3σ) for printing 32 nm and 22 nm modules, using the then state of the art resist – SEVR40. Subsequently, the same exposures were repeated with Gremlin 1 reticle when a new and improved resist—SEVR139—became available. Although this resist was able to resolve the 16 nm module, it did suffer from rather high line edge roughness (~ 8nm, 3σ). The last set of wafer exposures were done with Gremlin2 reticle, using SEVR139 resist. The printed wafers were inspected with KLA 2800 and KLA2825 tools, using die-to-die inspection methodology. Repeater analysis of defects on the wafer afforded the ability to select and inspect only defects occurring in the same corresponding location in multiple dies of the wafer; these defects were thus classified as the printable defects. SEM review of the printed wafer was done on the mask repeater defects with KLA eDR5000 tool.

3. RESULTS AND DISCUSSIONS

3.1 Blank Inspection and SEM Review Results

Shown in Figure 3 are the defect maps of Gremlin1 and Gremlin2 mask blanks, with total defect densities of 1.3 defects/cm^2 and 0.25 defect/cm^2, respectively, obtained with DF-40X tool.

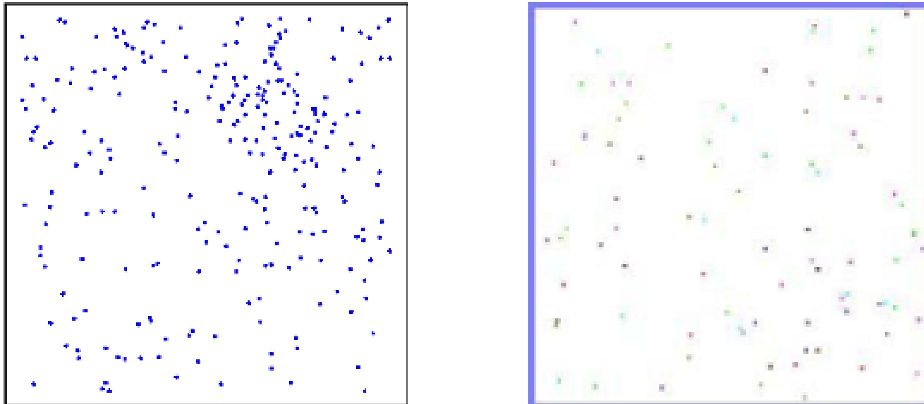

Gremlin1 mask blank Gremlin2 mask blank

Figure 3. Defect maps of Gremlin 1 and Gremlin 2 mask blanks with total defect densities of 1.3 defects/cm^2 and 0.25 defect/cm^2, respectively, as measured on the DF-40X tool.

Downloaded from SPIE Digital Library on 31 Mar 2010 to 192.146.1.254. Terms of Use: http://spiedl.org/terms

3.2 Reticle Inspection Results

Figure 4 shows blank and reticle defect inspection results obtained on Gremlin1 and Gremlin2 reticles. While the blank inspection was done with Siemens DF-40X tool, Gremlin 1 inspection was done with KLA-Tencor TeraScanHR tool with 257 nm illumination wavelength, while Gremlin2 inspection was done with KLA-Tencor Teron 6xx tool. While the KLA-Tencor TeraScanHR tool detected 9 defects that originated from a total of 249 blank defects on the entire Gremlin1 reticle, the state-of-the-art KLA-Tencor Teron 6xx tool detected 18 blank defects that originated from total blank defects of 49. These results indicate that the state of the art Teron 6xx series inspection tool can detect a much larger fraction (10×) of the blank defects than TeraScanHR (the previous generation tool). While it is possible that some blank defects may have been covered during reticle patterning, it is also possible that the reticle patterning process may have added some defects.

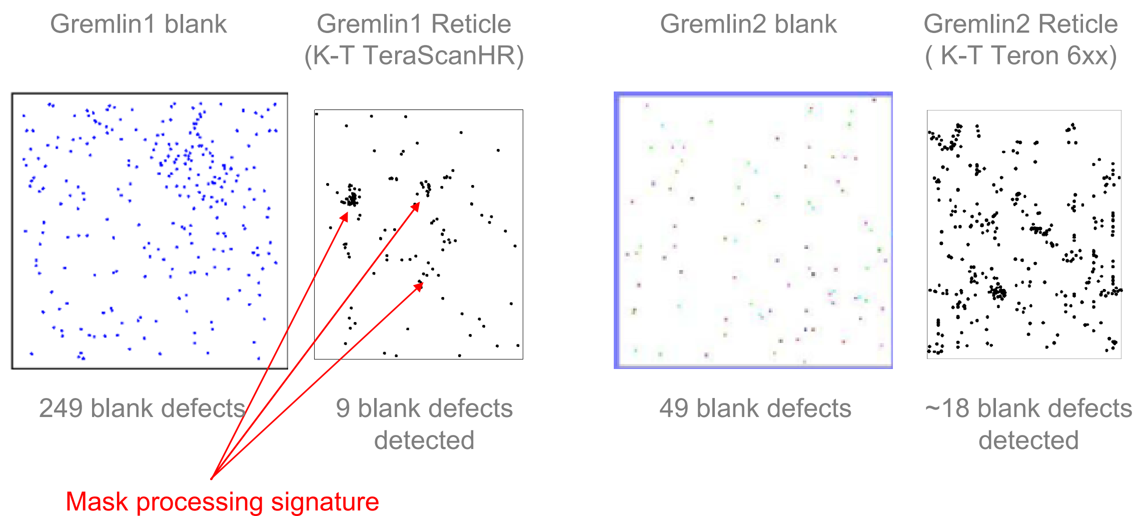

Figure 4. Gremlin1 and Gremlin2 blank and reticle defect inspection maps, showing the number of defects detected by the different inspection tool. The blanks were inspected with Lasertec tool, while Gremlin1 reticle was inspected with KLA-Tencor TeraScanHR tool, Gremlin2 reticle was inspected with KLA-Tencor Teron 6xx series tool.

Figure 5 shows examples of inspection images of blank defects detected on 16 nm and 22 nm modules of Gremlin2 reticle by the KLA-Tencor 6x series Teron tool, indicating good base pattern contrast, good signal from defects of interest, and reasonable background noise level, despite the significant noise from the reticle LER. The sensitivity of the Teron tool was reduced significantly from its potential maximum value due to the significant LER of the reticle features. It should be pointed out that sensitivity of this tool was optimized for the 16 nm module, and not for the other modules of Gremlin2.

Downloaded from SPIE Digital Library on 31 Mar 2010 to 192.146.1.254. Terms of Use: http://spiedl.org/terms

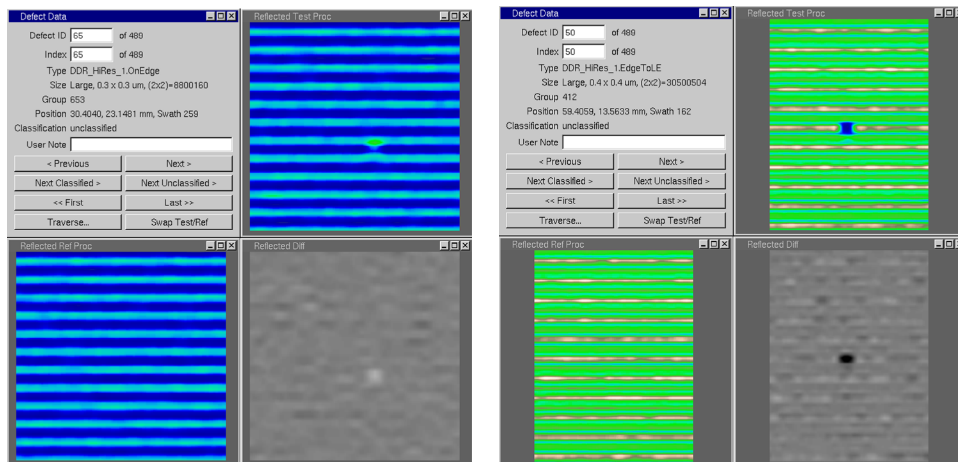

16 nm module 22 nm module

Figure 5. Examples of inspection images of blank defects detected on 16 nm and 22 nm modules of Gremlin2 reticle by the KLA-Tencor 6x series Teron tool.

Figures 6 and 7 show comparative defect maps between the Gremlin2 reticle inspection defects and the mask blank inspection defects, before and after the mask blank was processed at the mask house. These maps were generated with state of the art deep UV inspection tools (KLA-Tencor Teron 6xx series for reticle inspection and DF-40X for blank inspection), which appear to be more effective at detecting blank defects than previous generation tools. There is excellent correlation between the reticle inspection results and blank inspection result (after absorber deposition, just before e-beam litho step) (see Figure 7). A comparison of the blank defect map before (Figure 6) and after (Figure 7) absorber deposition reveals that many defects were in fact added at the absorber deposition step of the mask fabrication process.

Downloaded from SPIE Digital Library on 31 Mar 2010 to 192.146.1.254. Terms of Use: http://spiedl.org/terms

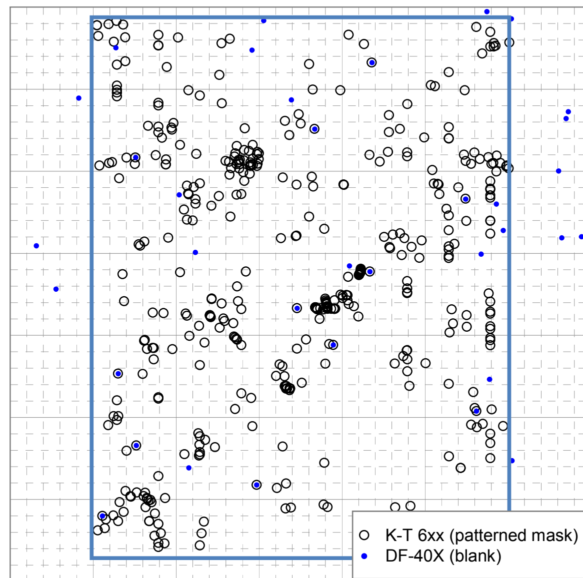

Figures 6 Comparative defect maps between the Gremlin2 reticle inspection defects and the mask blank inspection defects, before the mask blank was processed at the mask house.

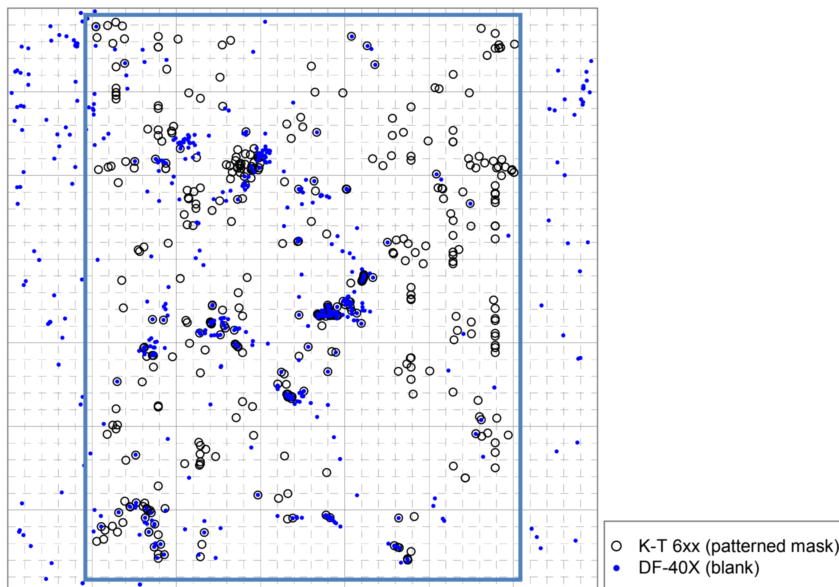

Figures 7. Comparative defect maps between the Gremlin2 reticle inspection defects and the mask blank inspection defects, after absorber deposition, but before electron beam patterning of the mask at the mask house.

Downloaded from SPIE Digital Library on 31 Mar 2010 to 192.146.1.254. Terms of Use: http://spiedl.org/terms

Figure 8 is a plot showing the dectectability of blank defects on patterned masks as a function of relative defect size (in terms of spherical equivalent volume diameter, SEVD). It appears that as relative blank defect size exceeds 0.1 of SEVD, the ability to detect it in grating-like features exceeds 50%.

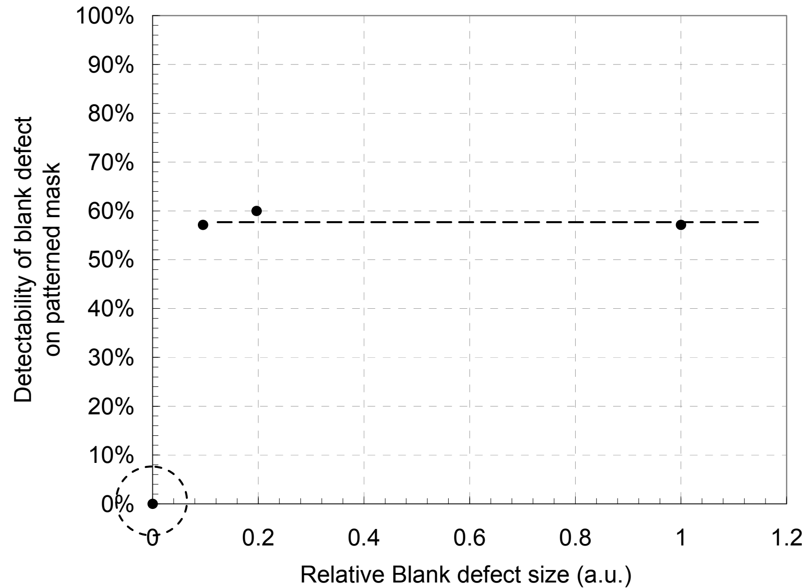

Figure 8. Detectability of blank defects as a function of relative defect size (in terms of spherical equivalent volume diameter).

3.3 Wafer Printing, Inspection and SEM Review Results

Shown in Figure 9 are plots of CD uniformity and line edge roughness as a function of slit position across an entire scanned exposure field that was exposed with Gremlin1 reticle, using SEVR40 resist, and highlighting a remarkably well controlled process for printing the 32 nm and 22 nm modules. The tight CD uniformity of 1.3 nm (3σ) and low LER of 3 nm (3σ) obtained for the serpentine and comb structures within the 32 nm and 22 nm modules helped to reduce roughness-related interference effects that may degrade the sensitivity of the inspection tools in capturing mask defects. This resist was however not able to resolve the 16 nm module. Although the SEVR139 resist process was able to pattern the 16 nm module, it did suffer from poor CD uniformity (~ 8nm, 3σ).

Downloaded from SPIE Digital Library on 31 Mar 2010 to 192.146.1.254. Terms of Use: http://spiedl.org/terms

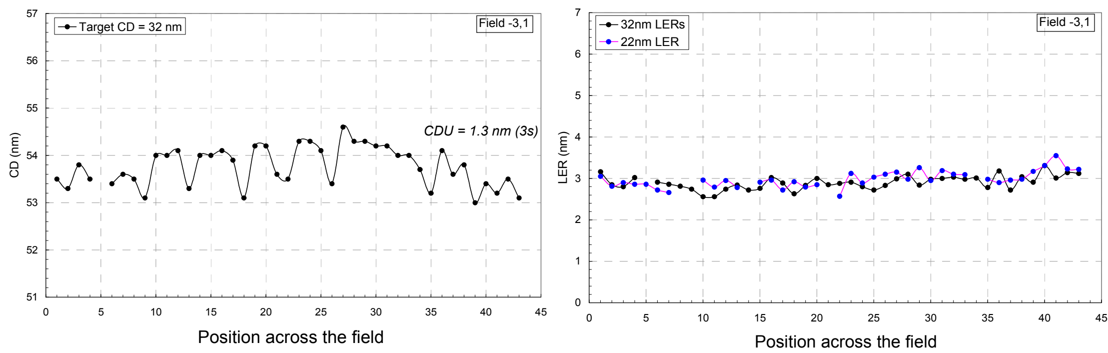

Figure 9. CD uniformity and line edge roughness as a function of slit position across an entire scanned exposure field that was exposed with Gremlin1 reticle, using SEVR40 resist

Figure 10 are defect maps of different modules of Gremlin1 mask repeater defects on a wafer patterned with with SEVR139 resist. The general trend in the defect densities in this Figure suggests that mask repeater defects become more printable as the pitch of the pattern gets smaller.

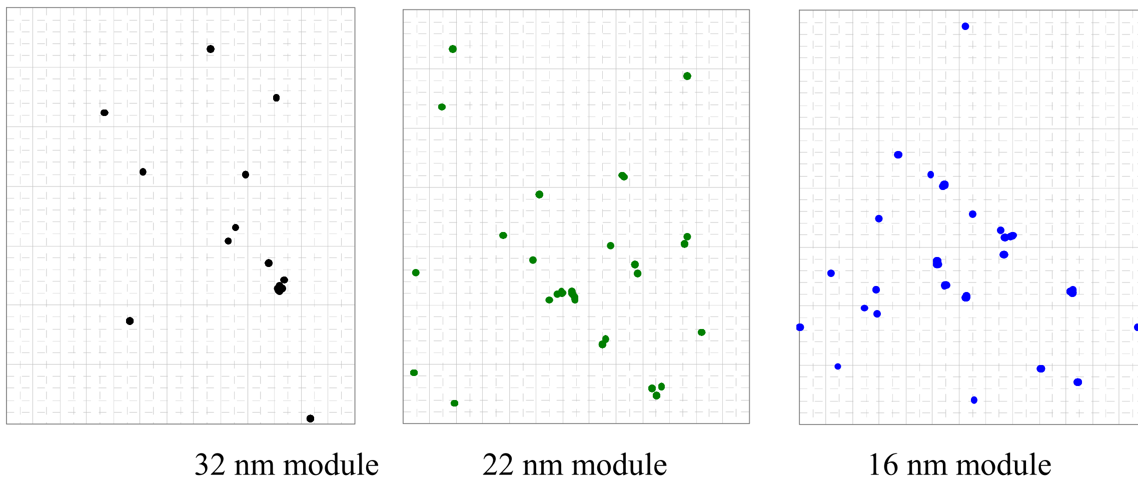

32 nm module 22 nm module 16 nm module

Figure 10. Defect map of different modules of Gremlin1 mask repeater defects on a wafer patterned with with SEVR139 resist. The number of repeater defects in the 32 nm, 22 nm and 16 nm modules were 14, 31 and 38, respectively.

Figure 11 shows Gremlin1 reticle defect map and wafer repeater defect map. There is a good correlation between the reticle defects and wafer repeater defects, which suggest that the wafer repeater defects are indeed reticle defects that were printed on the wafer. There is also a good correlation between the defect

Downloaded from SPIE Digital Library on 31 Mar 2010 to 192.146.1.254. Terms of Use: http://spiedl.org/terms

maps generated by the 257 nm wavelength inspection tool and 197 nm inspection tool.

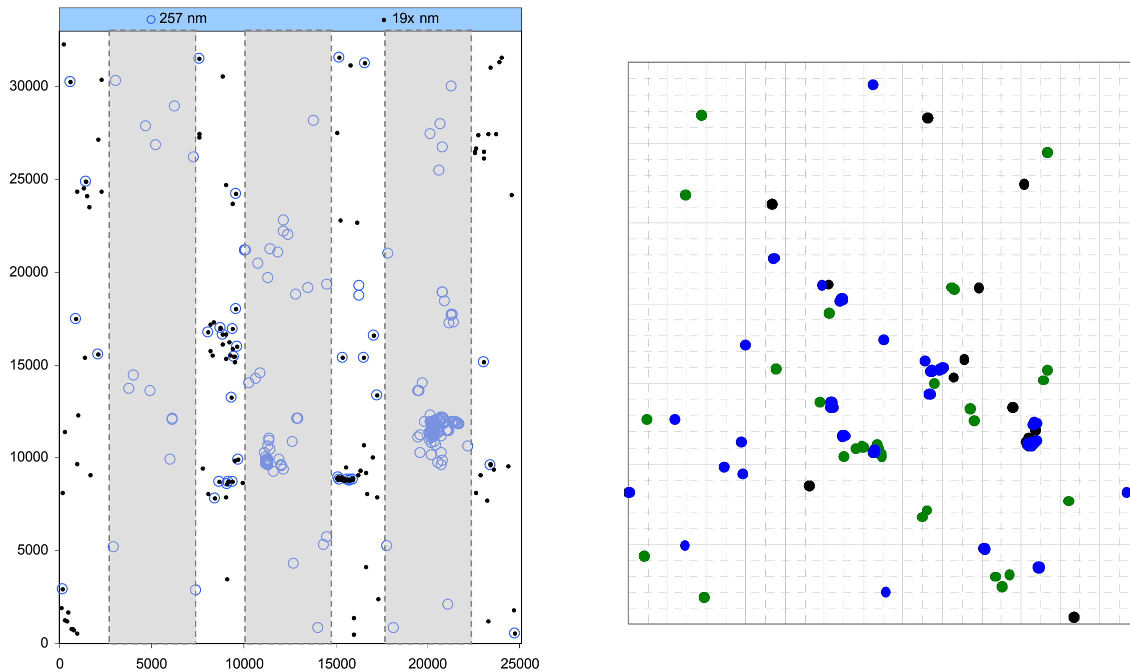

A. Reticle inspection B. Wafer inspection

Figure 11. Reticle and wafer repeater defect maps. The correlation between the defect maps generated by the 257 nm wavelength inspection tool and 197 nm inspection tool is shown in Figure A. The wafer was exposed with SEVR139 resist.

Figure 12 shows sample SEM images of printable Gremlin2 reticle defects on the wafer. Bridged patterns constitute most of the observed Gremlin 2 reticle printable defects observed on the wafer.

Downloaded from SPIE Digital Library on 31 Mar 2010 to 192.146.1.254. Terms of Use: http://spiedl.org/terms

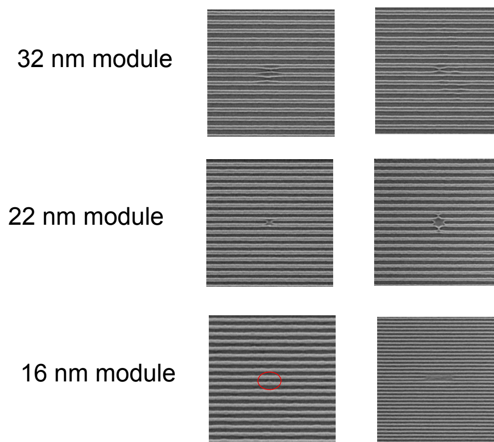

Figure 12. Sample SEM images of printable Gremlin2 reticle defects on the wafer

4. SUMMARY

Our studies on the printability of EUV mask defects down to a pitch of 56 nm shows a trend of increased printability as the pitch of the printed pattern gets smaller – a well established trend at larger pitches of 80 nm and 104 nm, respectively. The sensitivity of state-of-the-art reticle inspection tools is greatly improved over that of the previous generation of tools. There appears to be no apparent decline in the sensitivity these state-of-the-art reticle inspection tools for higher density (smaller) patterns on the mask, even down to 56nm pitch (1×). The use of state-of-the-art inspection tools is essential for obtaining a clear assessment of current EUV mask readiness for pilot line production. Our preliminary results indicate that a blank defect density of the order of 0.25 defects/cm^2 as in Gremlin2 reticle can support very early learning on EUV pilot line production at the 16 nm node.

5. ACKNOWLEDGMENTS

The authors would like to acknowledge the useful inputs from Harry J. Levinson of GLOBALFOUNDRIES, M. Yokoyama, Y. Ikuta, and M. Komakine of Asahi Glass Company. The authors would also like to acknowledge the assistance of Hiro Mizuno of Toshiba and the ASML EUVL team in Albany. Part of this work was performed by the Research Alliance Teams at IBM Research and Development Facilities in Albany, NY

Downloaded from SPIE Digital Library on 31 Mar 2010 to 192.146.1.254. Terms of Use: http://spiedl.org/terms

6. REFERENCES

[1] Mask defects can be defined as imperfections that result in critical dimension variations greater than a defined limit within a specific process window. See for example R.J. Socha, A.R. Neureuther, R. Singh, "Photomask Technology and Management," *Proc. SPIE*, **vol. 2087**, p. 277 (1993)

[2] B. La Fontaine, A. Tchikoulaeva, U. Okoroanyanwu, O. Wood, P. Ackman, C. Holfeld, K. Bubke, J.-H. Peters, S. Kini, S. Raghunathan, C. Boye, M. Yokoyama, Y. Ikuta, M. Komakine, "Assessing EUV Mask Defectivity," International Symposium on EUV Lithography, Prague (2009)

Downloaded from SPIE Digital Library on 31 Mar 2010 to 192.146.1.254. Terms of Use: http://spiedl.org/terms